Colloids and Surfaces A: Physicochemical and Engineering Aspects 675 (2023) 132005

Contents lists available at ScienceDirect

Colloids and Surfaces A: Physicochemical and Engineering Aspects

journal homepage: www.elsevier.com/locate/colsurfa

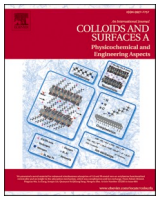

Chemically reduced graphene oxide based aerogels - Insight on the surface and textural functionalities dependent on handling the synthesis factors

Maksymilian Plata-Gryl [a,*,1], Roberto Castro-Muñoz [b,c,2], Grzegorz Boczkaj [b,d,**,3]

[a] Department of Process Engineering and Chemical Technology, Faculty of Chemistry, Gdansk University of Technology, Narutowicza St. 11/22, Gdansk 80-233, Poland
[b] Department of Sanitary Engineering, Faculty of Civil and Environmental Engineering, Gdansk University of Technology, Narutowicza St. 11/22, Gdansk 80-233, Poland
[c] Tecnologico de Monterrey, Campus Toluca, Eduardo Monroy Cárdenas 2000 San Antonio Buenavista, 50110 Toluca de Lerdo, Mexico
[d] Advanced Materials Centre, Gdansk University of Technology, Narutowicza St. 11/22, Gdansk 80-233, Poland

HIGHLIGHTS

- Step forward in properties control and "tailored" rGOAs engineering.
- Free surface energy depends only on GO dispersion concentration for rGOAs synthesis.
- Highest aerogels hydrophobicity is promoted by low GO dispersion concentration.
- Higher freezing temp. of hydrogel promote aerogels with lower surface area.
- Increased aerogel's surface roughness obtained in higher freezing temp. of hydrogel.

GRAPHICAL ABSTRACT

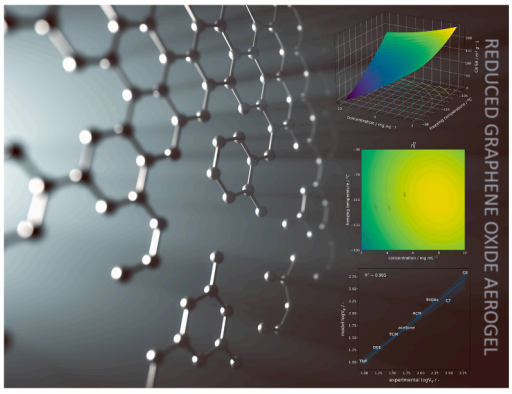

ARTICLE INFO

Keywords:
3D materials
Adsorption
Isomers separation
Nanomaterials
Sol-gel method
Surface science

ABSTRACT

Efficient adjusting of reduced graphene oxide aerogels properties requires information about experimental factor-aerogel property relationship. In this work, the reduced graphene oxide aerogels surface and textural functionalities in relation to precursor concentration, gelation time and hydrogel freezing temperature were studied in detail, with the use of dynamic adsorption method of gaseous organic probes and experimental design. The precursor concentration and the hydrogel freezing temperature have the strongest influence on textural properties - a negative correlation with apparent surface area was observed. The highest value of 229.36 $m^2 g^{-1}$ was obtained for samples synthesized at the lowest concentration of precursor (2 mg mL^{-1}) and hydrogel freezing temperature (−196 °C). Low precursor concentration promote formation of more hydrophobic aerogels.

* Correspondence to: Gdansk University of Technology, Faculty of Chemistry, Department of Process Engineering and Chemical Technology, G.Narutowicza St. 11/12, Gdansk 80-233, Poland.
** Correspondence to: Gdansk University of Technology, Faculty of Civil and Environmental Engineering, Department of Sanitary Engineering, G.Narutowicza St. 11/12, Gdansk 80-233, Poland.
E-mail addresses: maksymilian.plata-gryl@pg.edu.pl (M. Plata-Gryl), grzegorz.boczkaj@pg.edu.pl (G. Boczkaj).
[1] 0000–0001-5031–2908
[2] 0000–0002-7657–3302
[3] 0000–0002-5874–7591

https://doi.org/10.1016/j.colsurfa.2023.132005
Received 15 May 2023; Received in revised form 19 June 2023; Accepted 3 July 2023
Available online 5 July 2023

All aerogels display tendencies for dispersive, dipole-type and electron donor interactions. Moreover, a repulsion of electron lone pairs was observed, as well as shape-based selectivity (originating from porosity and surface roughness) in gas-solid adsorption process. Analysis of the free surface energy revealed that the maximum value (193.21 mJ m^{-2}) is obtained at 7.2 mg mL^{-1} precursor concentration, − 104 °C hydrogel freezing temperature and 23 h gelation time. Presented findings can translate directly into reduced graphene oxide aerogels tailored for specific applications such as adsorption or catalysis.

1. Introduction

Reduced graphene oxide aerogel (rGOA) is a lightweight, 3D material composed of reduced graphene oxide (rGO) flakes with highly interconnected porous structure, low density, and good chemical and thermal stability. It is one of the most interesting candidates for transferring outstanding properties of the graphene to 3D macroscopic objects, applicable in different fields [1–3]. The uniqueness of rGOA among other carbon materials stems from its high void volume (up to 99%) and open hierarchical pore network [1,4].

A variety of methods and procedures can be used for the fabrication of rGOAs, as reported recently in several reviews [5–7]. These methods can be divided into template and non-template based. Among non-template-based approaches for rGOA synthesis, the sol-gel methods based on reduction induced self-assembly of GO are recognized as a straightforward and versatile option for rGOA production. Upon elimination of oxygen functional groups, the conjugated aromatic structure of graphene is restored, resulting in a decreased electrostatic repulsion and interlayer distance - driven by the enhanced π-π stacking and hydrophobic effect, rGO flakes assemble into 3D hydrogel with water molecules enclosed within its structure [3,8,9].

The process is affected by different factors such as concentration of GO dispersion [10,11], GO flake size [12,13], gelation temperature and time (typically between 2 and 48 h) [14], type of reductant [10,15], and method of water removal from hydrogel [14,16]. Generally, GO concentrations between 1 and 10 mg mL^{-1} are used [14] but its effect is not completely clear. For samples reduced with dopamine a higher value of the surface area was observed, when more concentrated GO dispersions were used [10], whereas for aerogels self-assembled with the use of $NaHSO_3$, the opposite behaviour was observed [17].

For hydrogel drying, freeze-drying is commonly used. Because during the freezing of hydrogel graphene sheets are compressed by ice crystals and stacked together forming the cells and walls of rGOA [18,19], the process gives an unique possibility to control the porous structure through the regulation of the growth pattern of ice crystals. [20–22].

The reduction of the GO can be induced by high temperature and elevated pressure (solvothermal reduction) [23], chemical reductant (chemical reduction) [14], or solvothermal reduction promoted by addition of reductant [24]. Reductant is used to ease the temperature and pressure conditions required for hydrogel formation. Conventional reductants such as hydrazine or $NaBH_4$ are ineffective because gaseous by-products distort the rGOA structure (not to mention their high toxicity) [4,11]. As more environmentally friendly reductants, *l*-ascorbic (LAA) acid [4,24], ethylenediamine (EDA) [3] and $NaHSO_3$ [25] are commonly used. Other examples of reductants include dopamine [26], melamine [27], urea [28] or iodides [29]. High number of available reductant gives various options for tailoring aerogels properties, because reductants can also modify the surface by doping heteroatoms [30], providing additional crosslinking [25], or act as spacers preventing restacking of rGO sheets [31].

Sol-gel methods give a tremendous flexibility in regulating aerogels properties, but transparent correlations between properties and synthesis conditions are required. To date, there are relatively few works establishing systematic correlation between rGOA properties and synthesis conditions. In this work, we investigated surface properties of unmodified chemically reduced aerogels in relation to selected synthesis factors (GO concentration, gelation time and hydrogel freezing temperature). LAA was selected as a reductant because it has similar deoxygenation efficiency as a benchmark reductant (hydrazine). Additionally, it contains only carbon, oxygen and hydrogen, thus there is no risk of unintentional doping with heteroatoms [4]. For the analysis of rGOA samples, the inverse gas chromatography (IGC) technique was used, which was selected by the particular interest in the surface and interface properties.

2. Experimental

2.1. Graphene oxide (GO) synthesis

GO was synthesised according to the Tour's method [32]. Basically, graphite powder (synthetic, 7–11 μm, 99%, Alfa Aesar) was mixed with sulfuric (min. 95%, pure p.a., POCH) and orto-phosphoric acid (85%, pure p.a.-basic, POCH) in 1 L round bottom flask. The ratio of graphite to H_2SO_4 to H_3PO_4 was 1 g: 120 mL: 15 mL. Afterward, 6 g of $KMnO_4$ (pure p.a., POCH) were gradually added. The flask was cooled with ice bath to avoid excessive heating during $KMnO_4$ addition (the temperature was kept below 20 °C). Subsequently, the mixture was heated for 12 h at 50 °C and then cooled down to room temperature. Mixing and heating was provided by MS-H-Pro^T magnetic hot plate stirrer (Chemland).

The oxidation step was stopped by addition of 250 mL of ice-cold water (ultrapure Type I, provided by Direct-Q® 3UV-R system, Merck Millipore). Additionally, 3 mL of H_2O_2 (30%, pure p.a., POCH) were added to reduce manganese ions into soluble manganese sulphate. It resulted in colour change of the mixture from dark brown/black to bright yellow. The supernatant was decanted, fresh ultrapure water was added, and mixture was left for equilibration overnight. The washing process was repeated until the supernatant reached neutral pH. Residual water was removed by rotary evaporator (Rotavapor R-300, Buchi) at 30 °C (20 mbar, 50 RPMs) to avoid thermal reduction of oxygen functional groups on the surface of graphite oxide.

Since obtained graphite oxide may contain unoxidized graphite, it needs to be exfoliated to produce complete GO, therefore it was submitted to ultrasounds - 2 g of graphite oxide were mixed with 200 mL of ultrapure water and the mixture was then ultrasonicated twice for 15 min at 200 W using ultrasonic probe (Hielscher UP400St, 24 kHz, radiation area 2.2 cm^2). During ultrasonication the flask with mixture was kept in the cooling bath to avoid overheating and reduction of oxygen functional groups. Resulting dispersion was set aside in refrigerator overnight to settle out the unoxidized/unexfoliated graphite oxide. Remaining suspension was decanted, and water was removed by evaporation, as described previously. Obtained solid was labelled as GO and was used as precursor for aerogels synthesis. Table 1 presents the amount of different oxygen containing groups detected on the GO surface by the Boehm titration. The experimental procedure of titration is described in the supplementary information (**Text S1**).

Table 1
Amount of oxygen containing groups on the GO surface determined by Boehm titration.

Sample	acidic [mmol g^{-1}]			basic [mmol g^{-1}]
	phenolic	lactonic	carboxylic	
GO	NA	0.401 ± 0.048	2.570 ± 0.003	0.855 ± 0.004

2.2. Preparation of reduced graphene oxide aerogels (rGOA)

rGOA samples were prepared by a two-step process – hydrogel formation by chemical reduction of GO, and subsequent freeze-drying. The LAA (pure p.a., Chempur) was used as reductant and its ratio to GO was fixed at 4:1 by mass. As significant experimental factors the GO concentration, the reduction time and the hydrogel freezing temperature were selected. Their effect (main, interaction, and quadratic effects) on surface properties of aerogels were explored based on the Box-Behnken design [33], which requires less experiments than *e.g.* central composite design (CCD). Experimental factors with their values are presented in Table 2. A total of 15 experiments were executed (3 central points) - the detailed description of experimental conditions is shown in Table S1.

To produce hydrogels, GO dispersion (10 mg mL^{-1}) was mixed in glass containers with LAA dissolved in ultrapure water until obtaining desired concentration of GO and corresponding LAA to GO ratio. The samples were then placed in an oven, and the reduction process was carried out for a specified time at 95 °C. As a result, black monoliths (hydrogels) were obtained. To remove impurities hydrogels were washed with ultrapure water several times.

Water was removed from hydrogels by freeze-drying. Samples of hydrogels were frozen at different temperatures by immersion in liquid nitrogen (−196 °C) or in ethanol/liquid nitrogen cooling baths (for temperatures of −116 ± 2 and −36 ± 2 °C). Temperature of cooling baths was monitored by a resistance temperature detector. The sublimation process was carried out in freeze-drying chamber at a pressure below 20 Pa provided by rotary vacuum pump RV8 (Edwards). The pressure and drying endpoint were controlled by Pirani-type vacuum gauge VMV-1 (Value).

For statistical calculations, the R programming language and rsm package (version 2.10.2) were used [34]. Particularly, a model allowing to estimate the linearity, interaction, and quadratic or curvature effects, was generated by fitting the following polynomial to experimental data, as follows:

$$Y = \beta_0 + \sum_{i=k}^{k} \beta_i x_i + \sum_{i=k}^{k} \beta_{ii} x_i^2 + \sum_{i=1<}^{k} \sum_{j=1}^{k} \beta_{ij} x_i x_j + \varepsilon \quad (1)$$

where Y is the response, β_0 is the intercept, β_i and β_{ii} are the regression coefficients, and x_i and x_{ij} are the independent variables in their coded (−1, 0, 1) form. Terms x_i^2 and $x_i x_j$ describe quadratic and interaction terms, respectively. To estimate the goodness of fit of a model, the mean absolute error (MAE) and the mean absolute percentage error (MAPE) were used.

2.3. Fourier-transform infrared spectroscopy

Chemical structure of rGOAs was analysed by Fourier-transform infrared spectrophotometer Nicolet IR200 (Thermo Scientific, USA) using the attenuated total reflection (ATR) sampling technique. Data was collected in the range of 4000–400 cm^{-1} with 1 cm^{-1} resolution and processed in Spectragryph software [35].

2.4. Inverse gas chromatography

Inverse gas chromatography analyses were performed using Autosystem XL gas chromatograph (Perkin Elmer) equipped with a flame ionization detector (FID). Samples of rGOA were placed in stainless steel columns (5 cm length, 3.62 mm i.d.) with both ends plugged with a silane-treated glass wool (50MGS, Hewlett Packard). A list of columns with exact masses of rGOA samples used for measurements can be found in Table S1. Prior to analysis, columns were conditioned twice in the flow of a nitrogen carrier gas (N5.0, Linde Gas) under temperature program (10 min @ 50–5 °C min^{-1} – 120 min @ 250 °C), to remove residual contaminants.

IGC experiments were performed under a nitrogen flowrate of 20 mL min^{-1} at a temperature of 100 °C. The flowrate was controlled at the outlet from the column by a GFM Pro Flowmeter (Thermo Scientific). Additionally, it was corrected for compressibility of the gas and temperature of the column. Injector and detector temperatures were set to 250 °C.

The list of solutes used as molecular probes included: C_6 – C_9 n-alkanes, *iso*octane (*iso*C8), *cyclo*octane (*cyclo*C8), trichloromethane (TCM), tetrahydrofurane (THF), diethylether (DEE), ethyl acetate (EtOAc), acetonitrile (ACN) and acetone. Methane was used as non-interacting gas to make correction for void volume. More information about test probes can be found in Table S2. Each probe was injected at least two times, with 1 μL non-dead volume microsyringe (VWR), to ensure reproducibility of injection.

The volume of injections of each probe varied from 0.1 to 1 μL. It enables to perform IGC analyses at finite concentration (FC) using elution characteristic point method (ECP). All calculations including desorption isotherms, adsorption potential distribution, BET surface area values, morphology indices, dispersive and specific components of the surface free energy, electron donor and electron acceptor parameters were done using a self-made software, which was developed in Python programming language. Since the values of calculated parameters depend on surface coverage (θ), in this work they are reported for θ = 0.05, unless otherwise indicated. Detailed procedures and equations used for calculations can be found in Text S2.

3. Results and discussion

The importance of experimental factors for measured surface functionalities is presented in Table S3, as p-values. For the interpretation of results, a significance level of at least 0.1 was selected to declare that relationship between surface functionality (response) and given experimental factor is statistically significant. Fig. 1 presents a digital image of a GO dispersion before gelation, a self-assembled rGO hydrogel and a piece of a rGOA placed on a glass wool. The porosity of the rGOA sample was *ca.* 99% and the density was estimated to be *ca.* 26.5 mg cm^{-3}.

Table 2
Experimental factors with their levels for rGOA synthesis.

Factor		Level		
		-1	0	+ 1
Concentration [mg mL^{-1}]	X_1	2	6	10
Freezing temperature [°C]	X_2	-196	-116	-36
Gelation time [h]	X_3	6	15	24

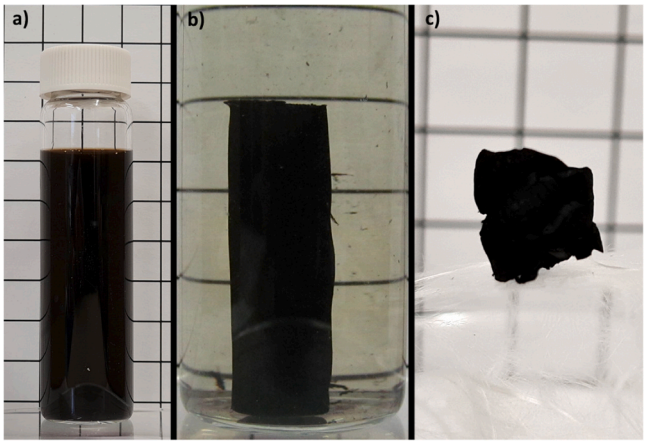

Fig. 1. a) precursor dispersion before gelation, b) self-assembled hydrogel after chemical reduction and gelation, c) a piece of rGOA placed on a glass wool fibres.

3.1. Chemical structure

The infrared spectrum of precursor (solid, before dispersing in water), presented in Fig. 2, displaying a typical profile for multi-layered GO. It is composed of three broad bands at 3000–3700 cm^{-1}, 1500–2000 cm^{-1} and 800–1500 cm^{-1}, which are the result of overlapping of vibrational modes of different infrared radiation absorbing moieties. As for the band at 3000–3700 cm^{-1}, it is attributed to hydroxyl groups, and since Boehm titration did not reveal the presence of phenolic groups, it is probably composed of absorption bands of C-OH of carboxyl groups and water intercalated between GO flakes. A strong adsorption band in the region of *ca.* 1720 cm^{-1}, together with signal below 3600 cm^{-1} is a clear sign of -COOH existence. Also, the contribution of lactols is possible in that region of the spectrum. Lack (or minimal) presence of phenols is supported by the fact that no shoulder or maximum is observed above 3600 cm^{-1} that could indicate presence of basal plane, or edge hydroxyls.

The part of the spectrum between 1650 and 1950 cm^{-1} originates from the overlapping of carboxyl and ketones vibrational modes (with ketone derivatives contributing mostly to the part above 1750 cm^{-1}), and by the asymmetric stretches (1550–1650 cm^{-1}) of the C═C carbons within the graphitic domains.

Broad bands in the fingerprint region (800–1500 cm^{-1}) are generated by the contribution of the different oxygen containing species. The maximum observed at *ca.* 1350 cm^{-1}, together with relatively small shoulder at *ca.* 860 cm^{-1}, provides a strong evidence for the presence of epoxides. To the signal in the frequency range 800–1330 cm^{-1} ether bonds can contribute, as well as five-membered ring lactols (950–1185 cm^{-1}).

Results of the FTIR analysis and Boehm titration confirm that the structure of the GO precursor is mainly formed from sp^2-hybridized carbon lattice, heavily decorated with carboxylic groups. This structural arrangement is indispensable for the synthesis of aerogels *via* chemical reduction method. As can be seen in Fig. 2, the contribution of the oxygen containing functionalities to IR spectrum decreases significantly once the gelation is finished. Concurrently, FTIR analysis indicate that residual oxygen functionalities are still present, which are crucial for hydrogel formation as they bind water molecules *via* hydrogen bonds. To further enhance the reduction, rGOA samples can be annealed in reducing atmosphere to remove residual oxygen functionalities.

To estimate quantitatively the reduction degree, the calculation method based on FTIR spectrum was used [36]. Basically, the amount of a given type of oxygen group was calculated by integration of FTIR spectrum. Following wavenumber ranges were used for carbonyl, hydroxyl and total oxygen, respectively: 880–1990, 3000–3700, 800–3700 cm^{-1}. GO used as precursor contained almost 70% of oxygen in form of C═O, 22% as C-OH, and 8% bonded in different configurations. For rGOA sample presented in Fig. 2, the total amount of oxygen dropped by 85%, and the contribution of carbonyl, hydroxyl and other forms of oxygen in remaining oxygen-containing functionalities was 73.7%, 15.2% and 11.0%, respectively. The decrease in C-OH contribution indicate that the carboxylic group has been reduced. On average, 73.3 ± 5.9% of oxygen groups were removed during synthesis, and the statistical analysis revealed that there was no significant difference in the reduction degree between prepared rGOAs. Fig. S1 presents the spectra for all synthesized rGOAs, while Table S4 enlists the contributions of different types of oxygen groups.

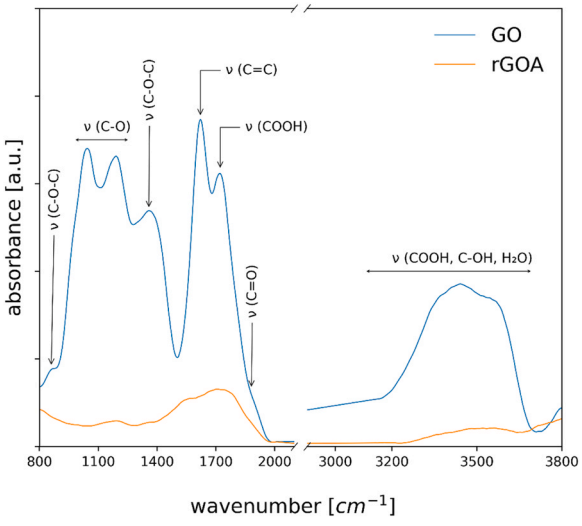

Fig. 2. Comparison of the IR absorption spectra of GO and rGOA.

3.2. Textural properties and surface morphology

Textural properties, such as accessible surface area of the material are relevant for numerous applications, *e.g.* separation processes. Herein, textural properties were evaluated by apparent surface area (*C8 SA*) - they were calculated from adsorption data of *n*-octane. Literature indicates that IGC analysis with organic probes can be used to estimate accessible surface area and it can demonstrate a good correlation with the standard method of low-temperature nitrogen adsorption [37]. This type of analysis is fast, easy and economical, especially when numerous samples have to be investigated.

Analysis of experimental results revealed that both the concentration of the precursor (p value < 0.0033) and freezing temperature (p value < 0.0029) of the hydrogel are highly significant for the textural properties of rGOA. As presented in Fig. 3, the analysis of the response surface indicates that there is a strong negative correlation with the concentration of the GO dispersion, and hydrogel freezing temperature – the lower the concentration and freezing temperature, the higher is the apparent surface area and porosity. The apparent surface area of all samples frozen at − 196 °C exceeded the value of 160 $m^2\ g^{-1}$, reaching as high as 230 $m^2\ g^{-1}$. Generally lower temperature suppressed the effect of GO concentration on the specific surface area values – coefficient of variability of *C8 SA* decreased from 60% to 45% as the temperature decreased from − 36 to − 196 °C. The lowest value of 7.51 $m^2\ g^{-1}$ was observed for sample frozen at − 36 °C (10 mg mL^{-1} dispersion concentration, 15 h gelation time). The MAE between experimental and calculated values for *C8 SA* was 14.87 $m^2\ g^{-1}$. Observed values are very similar to the ones reported in the literature and measured by low-temperature nitrogen adsorption [18,38,39].

The effect of hydrogel freezing temperature can be easily explained by the physics of ice - lower temperature increases the nucleation rate

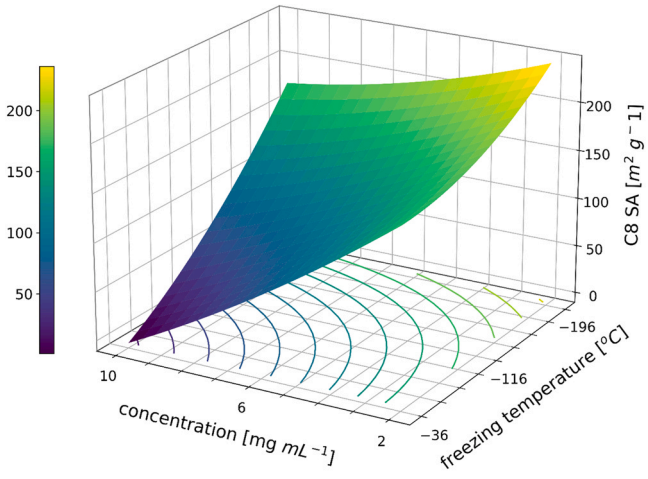

Fig. 3. Response surface for apparent surface area as a function of precursor concentration and hydrogel freezing temperature (slice at 15 h gelation time).

and restricts the ice crystal growth. As a result of a shorter crystallization time, smaller pores are produced within the rGOA structure upon sublimation of ice, yielding more porous monolith with enhanced apparent surface area. As mentioned previously, the effect of the precursor concentration on textural properties is uncertain. Data presented in this work provides strong evidence on negative correlation between surface area and precursor concentration. Low concentrations of precursor may promote the formation of more porous structure by preventing GO sheets restacking during gelation. Moreover, higher concentrations of precursor may restrict the formation of ice crystals. For GO it was observed that higher concentrations decrease their growth rate [40].

Experimentally, it was observed that the rGOA prepared from more concentrated GO dispersion was less fragile, because higher concentration results in more compact, layered structure and thicker walls of porous network. It is possible to achieve satisfactory textural properties with higher precursor concentrations (*e.g.,* $204.39 \pm 0.75\ m^2\ g^{-1}$ at concentration of 10 mg mL^{-1} and freezing temperature −196 °C), and it may be reasonable to sacrifice the surface area for enhanced mechanical, thermal and electrical properties. Additionally, gelation time was insignificant for prediction of *C8 SA* (p value = 0.1518).

Lower retention of branched or cyclic probe in comparison to its linear isomer indicates that its contact with the surface is hindered, revealing a nano/micro roughness of the surface (geometric heterogeneity). Aerogel samples were characterized by the *iso*octane and *cyclo*octane morphology index (*IM*), *i.e.* ratio of branched/cyclic alkane to linear alkane retention volume. The roughness of all rGOA samples is manifested by IM_{isoC8} and $IM_{cycloC8}$ values less than 1. For all samples, *IM values* increase with the surface coverage. Fig. 4 presents the retention volume of octane isomers for rGOA samples and theoretical selectivity between isomers, calculated for surface coverage $\Theta = 0.05$. On average, the retention of *iso*octane and *cyclo*octane was 5.9 and 4 times lower in comparison to *n*-octane, respectively. Moreover, there is also 30–40% difference between retention volume of *iso* and *cyclo*octane. This latter aspect indicates a possibility to use rGOAs for adsorptive separation of hydrocarbon isomers based on their limited accessibility to rGOA surface. Consequently, the highest selectivity was calculated for sample rGOA_4. The $nC_8/isoC_8$, $nC_8/cycloC_8$, and $cycloC_8/isoC_8$ selectivity values were 10.9 ± 0.12, 7.18 ± 0.30 and 1.52 ± 0.04, respectively. For that sample, the theoretical selectivity between heptane and *iso*octane (both compounds having similar boiling points *ca.* 98.4 and 99.0 °C, respectively) is 3.49. The clearly outlying values of specific retention volumes for rGOA_4, presented in the Fig. 4, are a result of its

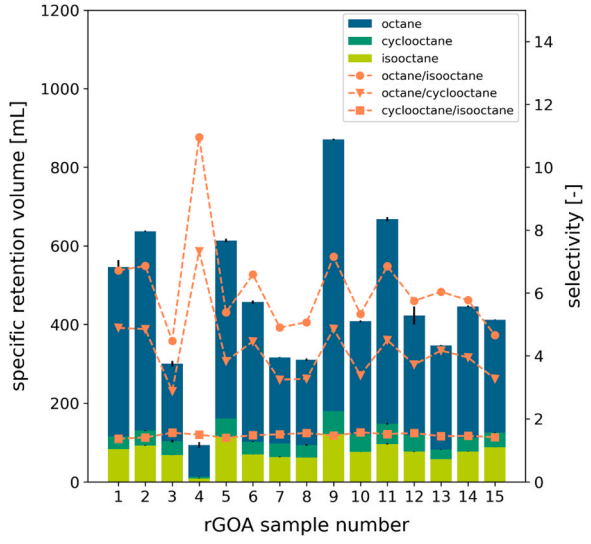

Fig. 4. Specific retention volume and selectivity of octane isomers measured for rGOA samples based on single component retention data. Bars for each probe are superimposed. Error bars represent standard deviations.

low surface area ($7.51\ m^2\ g^{-1}$, the lowest among rGOA samples prepared).

The relationship between experimental factors and morphology indices by response surface methodology revealed that hydrogel freezing temperature is the most determinative for *IM* value - as it increases, the IM_{isoC8} and $IM_{cycloC8}$ values also decrease. Response surfaces for these parameters can be found in Fig. S2. Upon freezing of hydrogel, GO sheets are compressed by ice crystals and stack together, along with the ice crystal growth direction, forming the walls of rGOA porous network. At lower temperatures, a higher number of small ice crystals is produced, which can act as spacers reducing the restacking of rGO sheets. Importantly, it promote also formation of smaller pores. On the contrary, higher freezing temperature will promote the formation of large crystals and stacking of multiple rGO sheets, thus leading to an increased roughness of the surface of the rGOA. The highest roughness ($IM_{isoC8} = 0.092$, $IM_{cycloC8} = 0.139$) was observed for sample rGOA_4 prepared at hydrogel freezing temperature of − 36 °C (10 mg mL^{-1} GO concentration, 15 h gelation time), whereas the lowest ($IM_{isoC8} = 0.227$, $IM_{cycloC8} = 0.344$) for sample rGOA_3 (−196 °C hydrogel freezing temperature, 10 mg mL^{-1} GO concentration, 15 h gelation time). Geometric heterogeneity of rGOAs surface combined with porosity provide the basis for selective separation of structural isomers in sorption based separation processes.

3.3. Surface free energy and intermolecular forces

Analysis of the surface free energy is essential for the characterisation of a material from the point of view of macroscopic properties such as dispersibility, wetting, adhesion/cohesion, static charge, conductivity, adsorption capacity among others. Thus, it plays an important role in different applications, *e.g.,* governing intermolecular interactions of catalysts or adsorbents.

The total surface free energy γ_S^T is typically divided into dispersive γ_S^D and specific γ_S^{SP} component. The dispersive part originates from long range of London forces, while specific originates from short range, polar (acid-base) interactions, including hydrogen bonding. The former one is non-specific, and γ_S^D value can be used as an indicator of general activity of a material. The analysis revealed that generally all parameters related to the surface free energy are dependent only on the concentration of GO dispersion used for synthesis of rGOA. Fig. 5 presents the response surfaces for γ_S^D, γ_S^{SP} and γ_S^T determined at a 0.05 surface coverage.

Collected data indicate that only the concentration of precursor plays an important role in the regulation of the surface free energy, and its components, of the rGOAs. Punctually, the dispersive part is the most prominent component of γ_S^T. It increases with increase of precursor concentration, reaching an optimum at *c.a.* 7.5 mg mL^{-1}. Higher concentrations of GO dispersion results in rGOA with lower value of the γ_S^D. The initial increase may be explained by higher number of rGO flakes and C═C bonds, interacting with test probes (alkanes), because dispersion contribution is directly related to the planar π-surface of the rGO. Subsequent decrease of the γ_S^D at higher concentrations of precursor may be linked to increased agglomeration/restacking and limitation of π-surface contact area with test probes. Such information may be important for the application of rGOA in nanoelectronics - noncovalent modification of graphene, through π-π stacking and dispersive interactions with aromatic molecules, is considered a promising method of electronic properties modification [41].

For a specific component, the optimum value (stationary point) was not observed within the experimental range of precursor concentration. The highest values were measured for rGOA prepared with the use of 10 mg mL^{-1} GO dispersion. As the concentration increases, there are more rGO flakes, and more specific adsorption centres to interact with polar probe molecules. The stacking of rGOA flakes may be less impactful, compared to γ_S^D, since the oxygen functional groups are predominantly located on edges of GO flakes [42]. It applies especially to

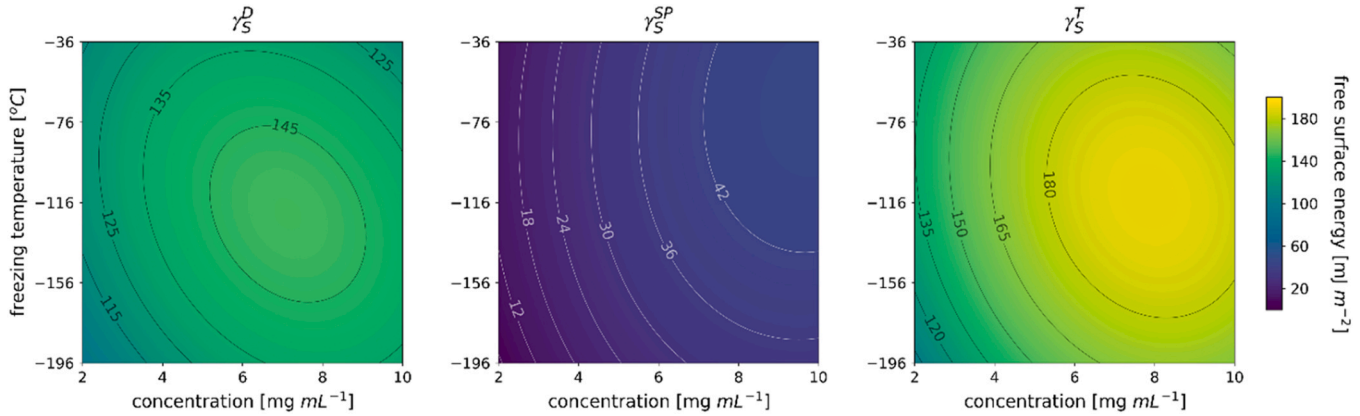

Fig. 5. Response surface analysis for free surface energy and its components (at $\Theta = 0.05$) as a function of precursor concentration and freezing time (slice at gelation time of 15 h). Dispersive (γ_S^D), specific (γ_S^{SP}), and total (γ_S^T).

carboxylic groups which are the most dominant in GO used for synthesis of rGOAs. Compared to γ_S^D, the γ_S^{SP} is few times lower indicating that dispersive interactions will dominate adsorbate-adsorbent interactions. The highest discrepancy ($\gamma_S^D/\gamma_S^{SP} = 20.2$) was observed for sample prepared with low concertation of GO dispersion (2 mg mL^{-1}), whereas the lowest ($\gamma_S^D/\gamma_S^{SP} = 2.4$) for sample synthesized from 10 mg mL^{-1} precursor concentration. Apart from the surface character, the relatively high values of γ_S^D observed for rGOA samples can be caused by high porosity/developed surface area. In small pores, with dimension close to molecular size of the probe, the test probe molecules can be affected by cooperative effect of opposite walls [43].

Since specific interactions of the solid surface are mainly responsible for interaction with polar molecules, it is possible to compare the hydrophilicity of a surface of a carbon material based on the hydrophilicity index *(HI), i.e.* ration of γ_S^{SP} to γ_S^T [44]. The higher its value, the lower its hydrophobicity, due to the contribution of the γ_S^{SP} to overall free surface energy being higher. This approach can be useful in case of porous samples because it is difficult to analyse them, for example, by water contact angle method. As the specific interactions itself, the (*HI*) exhibits strong correlation with the concentration of precursor ($p = 0.0097$). To prepare more hydrophobic surfaces, which will display lower affinity, *e.g.,* water molecules, a low concentration of GO dispersion should be used. This may be useful for the separation of gases by adsorption in humid conditions – additionally rGOA prepared from low GO concentrations exhibit also higher apparent surface area, which is crucial for adsorption capacity. The response surface for *HI* is presented in Fig. S3.

In IGC theory, the specific adsorbate-adsorbent interactions originate from their electron-donor (γ_S^-) and electron-acceptor (γ_S^+) properties. All rGOA samples exhibited a basic character of the surface ($\gamma_S^+/\gamma_S^- < 1$), and it was more distinct as the concentration of the precursor decreased. Thus, the surface of rGOAs will interact more favourably with acidic (electron-acceptor) compounds. The presence of specific (electron-donor and electron-acceptor) adsorption centres may be important from the point of view of the application in the *e.g.* catalysis field. The data for γ_S^-, γ_S^+, and γ_S^+/γ_S^- is presented in Fig. S4.

Over the course of experiments, adsorption data of a range of compounds was analysed, including alkanes and polar molecules with different acid-base properties (Table S2). By comparing the free energy of adsorption (ΔG_A) of a polar test probe and an alkane with similar molecular descriptor (*e.g.* topological index, X_T), a contribution of dispersive interactions can be estimated. Hence, the difference should arise from the specific interactions. All rGOAs samples demonstrated a very similar pattern of the specific part of the free energy of adsorption (ΔG_A^{SP}). Its value decreased in the following order: ACN > TCM/acetone > EtOAc > DEE > THF. This coincides quite well with their corrected Gutmann acceptor number (*AN**), which is a measure of the electrophilic properties of a molecule, *i.e.* ability to accept electrons [45]. It is another proof that the surface of analysed rGOAs is electron-donor (basic) in nature. The relationship between ΔG_A^{SP} and *AN** for rGOA_4 sample is presented in Fig. 6.

To explain the nature of specific interactions in greater detail, the Abraham solvation parameter model, presented in the Eq.(2), was fitted to retention data of test probes used for analysis.

$$\log V_g = eE + sS + aA + bB + lL + c \quad (2)$$

According to the model, the retention of a compound in a chromatographic system should be the sum of different types of interactions between adsorbate and adsorbent. From the perspective of adsorbent, these interactions are described by the following constants: e – tendency to π- and n-electron pairs interactions, s – ability to dipole-dipole interactions (dipolar/polarizable character of the surface), a and b are differences between adsorbent and mobile phase in hydrogen bond basicity and acidity, respectively, and l is the strength of dispersive interactions [46]. The uppercase letters are constants for test probes describing their ability for given interactions. The rGOA constants are presented in Table S5. Fig. 7 presents the predicted and experimental retention volume for rGOA_5 sample obtained by the model.

The analysis of the rGOA constants obtained by fitting the Abraham's LSER model to retention data of test probes revealed that all rGOAs samples have a negative value of e constants. It is not typical for adsorbents, however, such values are observed in gas chromatography for

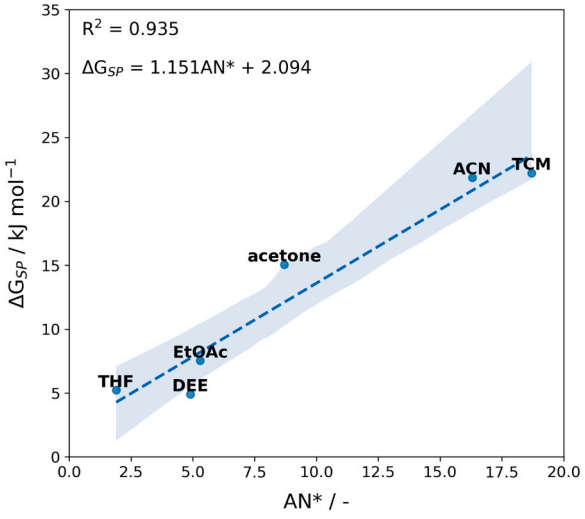

Fig. 6. Correlation between electrophilic properties of test probes and specific interactions with reduced graphene oxide aerogel surface (rGOA_4).

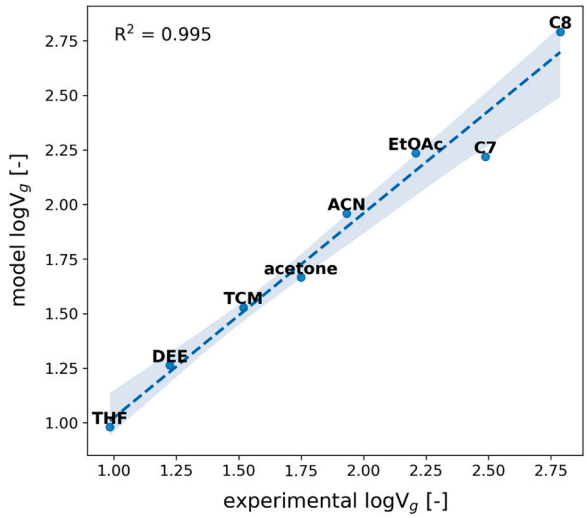

Fig. 7. Experimental and predicted values of $\log V_g$ by means of the Abraham's LSER model.

fluorine-containing stationary phases [47]. This behaviour originates in the method of the solute descriptors (*i.e., E,* excess molar refraction modelling the polarizability contribution to retention) determination using *n*-alkanes. The negative values indicate that the rGOAs structure is electronegative and make electrons less available for π- and *n*-electron pairs interaction. Moreover, $e < 0$ demonstrates that this type of interactions will lead to a decrease in the retention of test probes due to electron lone pair repulsion.

The lack of significance of *b* constant for prediction of retention of test probes, and simultaneously high values (and statistical significance) of constant *a* indicate that the surface of rGOAs is basic – without hydrogen-bond forming acidic adsorption centres. Limited hydrogen-bond acidity of rGOAs may point a direction for further studies to extend the selectivity of rGOAs, *e.g.,* in separation techniques, especially that a considerable variability in hydrogen-bond basicity is observed for many organic compounds. Constants *s* and *l* are both positive, indicating a contribution of dipole-type and dispersive interactions to the retention of test probes, respectively.

3.4. Adsorption potential distribution of rGOAs

The heterogeneity of the rGOAs surfaces was compared based on the *FWHM* of *n*-octane adsorption potential distribution. This part of the studies revealed that the surface of the adsorbent becomes more homogenous as the gelation time is prolonged. The minimal value was observed for 24 h. Fig. 8 presents the adsorption potential distributions of *n*-octane, chloroform, and ethyl acetate for selected samples. They depict the amount of adsorbate (μmol) adsorbed at the adsorption centre with a given adsorption potential (kJ mol^{-1}) per 1 g of adsorbent. The distributions were extrapolated outside potential values covered by experimental data based on split-Pearson VII distribution.

Presented distributions reveal that the number of adsorption centres detected by *n*-octane probe decreased with concentration. It is obviously linked to the lower surface area of aerogels synthesized from more concentrated precursor dispersions. Interestingly, the distribution for electron-acceptor and electron-donor polar probes (chloroform and ethylacetate) are very similar regardless of the concentration of GO used. It means that the reduction of the surface area does not affect specific adsorption centres to the same degree as dispersive ones. Possible explanation is that this type of adsorption centres may be located on the edges of rGO flakes, and stacking observed during aerogels formation does not limit the accessibility of test probes molecules to it significantly.

4. Conclusions

The inverse gas chromatography allowed to relate different surface properties (*e.g.,* dispersive and specific components of the surface free energy, adsorption potential distribution, electron-donor and electron-acceptor properties, surface morphology, textural characteristics, *etc.*) to synthesis conditions and revealed aerogels tendencies for specific molecular interactions. The goodness-of-fit of experimental and simulated values of aerogels parameters calculated in this work are presented in Fig. S5.

Experiments revealed that among the factors studied the precursor concentration and hydrogel freezing temperature have the strongest influence on aerogels properties. Especially, textural properties were strongly affected by these parameters - a negative correlation with apparent surface area was observed. The highest value of 229.36 $m^2 g^{-1}$ was obtained for samples synthesized at the lowest concentration of graphene oxide precursor (2 mg mL^{-1}) and hydrogel freezing temperature (−196 °C). Being aware of such dependence is important for tailoring aerogels toward adsorptive separations, especially wastewater and waste gas treatments where high surface area has a crucial role in process effectiveness.

Other molecular separation applications may rely more upon surface chemistry and morphology rather than surface area. Analysis of retention data of test probes provide an important insight on reduced

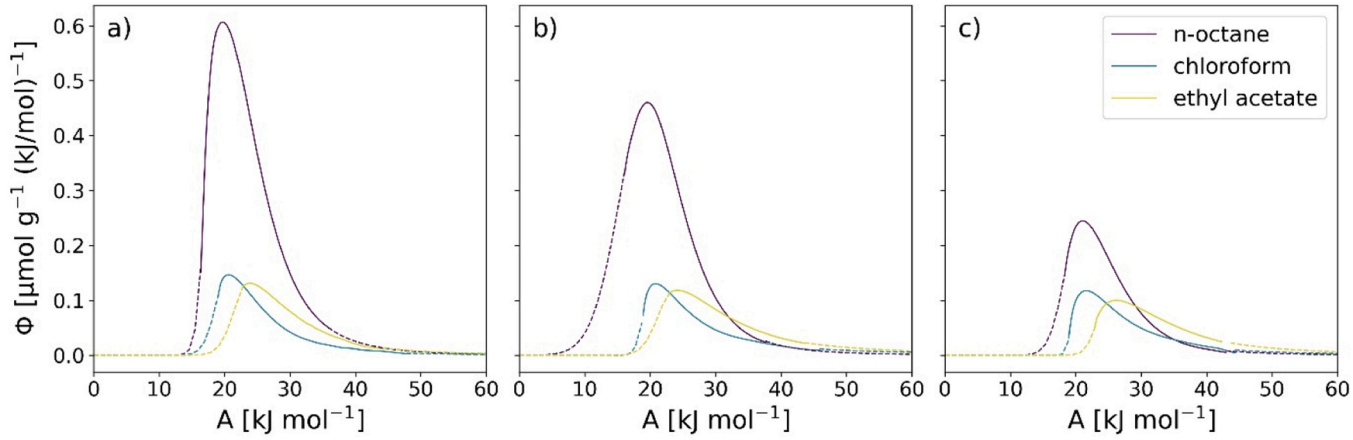

Fig. 8. Adsorption potential distribution for aerogels samples prepared at − 116 °C hydrogel freezing temperature and different concentrations: a) 2 mg mL^{-1}, b) 6 mg mL^{-1}, c) 10 mg mL^{-1}. Solid lines represent the part of distribution covered by experimental data. Dashed line is an extrapolation using split-Pearson VII distribution.

graphene oxide aerogels tendencies toward different molecular interactions. Among studied possibilities, the strongest were dispersive, dipole-type and electron-donor interactions. Interestingly, the uncommon (for gas-solid separations) effect of repulsion of electron lone pairs was observed. Abovementioned phenomenon can be used as starting point for selectivity optimization in gas-liquid and gas-solid separation techniques. Moreover, analysis of the retention of octane isomers revealed molecular level roughness of the surface, and selectivity based on shape in adsorption on reduced graphene oxide aerogel surface, which indicate a potential for structural isomers separation.

Apart from textural properties, the concentration of GO precursor had evident effect on the surface free energy of reduced graphene oxide aerogels. Its value increased with the increase of the concentration and reached maximum value at *c.a.* 7.2 mg mL (and at −104 °C hydrogel freezing temperature). Higher concentration resulted in decrease of the γ_S^T – the lowest value was measured for sample synthesized with 2 mg mL^{-1} graphene oxide dispersions (98.09 mJ m^{-2}). Similar pattern was revealed for dispersive component of γ_S^T, while for a specific component the maximum value (56.85 mJ m^{-2}) was at graphene oxide concentration of 10 mg mL^{-1}. The knowledge about the link between synthesis parameters and the surface free energy is crucial not only for direct application of reduced graphene oxide aerogels, but also for surface modification. It is important for adhesion in composites, catalytic and adsorption properties or wettability of the reduced graphene oxide aerogels. For example in nanoelectronics dispersive interactions with aromatic molecules can be an efficient method of noncovalent modification of electronic properties.

On the other hand, contribution of the γ_S^{SP} to γ_S^T may be used as a convenient comparator of hydrophilicity, especially for porous samples which are difficult to analyse with standard methods. To prepare more hydrophobic surfaces, which will display lower affinity, *e.g.,* water molecules, a low concentration of GO dispersion should be used. The lowest hydrophilicity index value (0.047) was determined for rGOA synthesized with 2 mg mL^{-1} graphene oxide concentration (−116 °C hydrogel freezing temperature and 6 h gelation time), while the most hydrophilic (HI = 0.295) was the rGOA synthesized at 10 mg mL^{-1} graphene oxide concentration (−116 °C hydrogel freezing temperature and 24 h gelation time).

Reported results provide extensive data useful to understand factors important for aerogels surface properties and can assist in the preparation of custom-made aerogels, for any application field where specific properties are required.

CRediT authorship contribution statement

Maksymilian Plata-Gryl: Conceptualization, Methodology, Investigation, Resources, Writing – original draft, Visualization, Project administration, Funding acquisition. **Roberto Castro-Muñoz:** Methodology, Writing – review & editing, Visualization, Supervision. **Grzegorz Boczkaj**: Conceptualization, Methodology, Resources, Writing – review & editing, Visualization, Supervision.

Declaration of Competing Interest

The authors declare that they have no known competing financial interests or personal relationships that could have appeared to influence the work reported in this paper.

Data Availability

The data that support the findings of this study are available in the Zenodo and Bridge of Knowledge open data repositories. DOI: 10.5281/zenodo.7712799.

Acknowledgments

Dr Maksymilian Plata-Gryl gratefully acknowledge the financial support from the National Science Centre, Cracow, Poland – Project PRELUDIUM18, no. UMO-2019/35/N/ST8/04226.

Appendix A. Supporting information

Supplementary data associated with this article can be found in the online version at doi:10.1016/j.colsurfa.2023.132005.

References

[1] E. Garcia-Bordejé, A.M. Benito, W.K. Maser, Graphene aerogels via hydrothermal gelation of graphene oxide colloids: fine-tuning of its porous and chemical properties and catalytic applications, Adv. Colloid Interface Sci. 292 (2021), https://doi.org/10.1016/j.cis.2021.102420.
[2] B. Guo, G. Liang, S. Yu, Y. Wang, C. Zhi, J. Bai, 3D printing of reduced graphene oxide aerogels for energy storage devices: a paradigm from materials and technologies to applications, Energy Storage Mater. 39 (2021) 146–165, https://doi.org/10.1016/j.ensm.2021.04.021.
[3] T.X. Trinh, D.M. Nguyet, T.H. Quan, T.N.M. Anh, D.B. Thinh, L.T. Tai, N.T. Lan, D. N. Trinh, N.M. Dat, H.M. Nam, M.T. Phong, N.H. Hieu, Preparing three-dimensional graphene aerogels by chemical reducing method: investigation of synthesis condition and optimization of adsorption capacity of organic dye, Surf. Interfaces 23 (2021), 101023, https://doi.org/10.1016/j.surfin.2021.101023.
[4] W. Chen, L. Yan, In situ self-assembly of mild chemical reduction graphene for three-dimensional architectures, Nanoscale 3 (2011) 3132–3137, https://doi.org/10.1039/c1nr10355e.
[5] M. Kotal, J. Kim, J. Oh, I.K. Oh, Recent progress in multifunctional graphene aerogels, Front Mater. 3 (2016) 1–22, https://doi.org/10.3389/fmats.2016.00029.
[6] G. Gorgolis, C. Galiotis, Graphene aerogels: a review, 2d Mater. 4 (2017), 032001, https://doi.org/10.1088/2053-1583/aa7883.
[7] Y. Xia, C. Gao, W. Gao, A review on elastic graphene aerogels: design, preparation, and applications, J. Polym. Sci. 60 (2022) 2239–2261, https://doi.org/10.1002/pol.20220179.
[8] D. Zhi, T. Li, J. Li, H. Ren, F. Meng, A review of three-dimensional graphene-based aerogels: synthesis, structure and application for microwave absorption, Compos B Eng. 211 (2021), 108642, https://doi.org/10.1016/j.compositesb.2021.108642.
[9] R. Singh, S. Ullah, N. Rao, M. Singh, I. Patra, D.A. Darko, C.P.J. Issac, K. Esmaeilzadeh-Salestani, R. Kanaoujiya, V. Vijayan, Synthesis of three-dimensional reduced-graphene oxide from graphene oxide, J. Nanomater 2022 (2022), https://doi.org/10.1155/2022/8731429.
[10] X. Song, L. Lin, M. Rong, Y. Wang, Z. Xie, X. Chen, Mussel-inspired, ultralight, multifunctional 3D nitrogen-doped graphene aerogel, Carbon N. Y 80 (2014) 174–182, https://doi.org/10.1016/j.carbon.2014.08.054.
[11] J.J. Shao, W. Lv, Q.H. Yang, Self-assembly of graphene oxide at interfaces, Adv. Mater. 26 (2014) 5586–5612, https://doi.org/10.1002/adma.201400267.
[12] Z. Xu, Y. Zhang, P. Li, C. Gao, Strong, conductive, lightweight, neat graphene aerogel fibers with aligned pores, ACS Nano 6 (2012) 7103–7113, https://doi.org/10.1021/nn3021772.
[13] W. Gao, N. Zhao, W. Yao, Z. Xu, H. Bai, C. Gao, Effect of flake size on the mechanical properties of graphene aerogels prepared by freeze casting, RSC Adv. 7 (2017) 33600–33605, https://doi.org/10.1039/c7ra05557a.
[14] S.T. Nguyen, H.T. Nguyen, A. Rinaldi, N.P.V. Nguyen, Z. Fan, H.M. Duong, Morphology control and thermal stability of binderless-graphene aerogels from graphite for energy storage applications, Colloids Surf. A Physicochem Eng. Asp. 414 (2012) 352–358, https://doi.org/10.1016/j.colsurfa.2012.08.048.
[15] Z. Tang, S. Shen, J. Zhuang, X. Wang, Noble-metal-promoted three-dimensional macroassembly of single-layered graphene oxide, Angew. Chem. - Int. Ed. 49 (2010) 4603–4607, https://doi.org/10.1002/anie.201000270.
[16] A.I. Pruna, A.C. Cárcel, A. Benedito, E. Giménez, The effect of solvothermal conditions on the properties of three-dimensional N-doped graphene aerogels, Nanomaterials 9 (2019) 350, https://doi.org/10.3390/nano9030350.
[17] Y. Cheng, S. Zhou, P. Hu, G. Zhao, Y. Li, X. Zhang, W. Han, Enhanced mechanical, thermal, and electric properties of graphene aerogels via supercritical ethanol drying and high-Temperature thermal reduction, Sci. Rep. 7 (2017) 1–11, https://doi.org/10.1038/s41598-017-01601-x.
[18] S. Wu, R.B. Ladani, J. Zhang, K. Ghorbani, X. Zhang, A.P. Mouritz, A.J. Kinloch, C. H. Wang, Strain sensors with adjustable sensitivity by tailoring the microstructure of graphene Aerogel/PDMS nanocomposites, ACS Appl. Mater. Interfaces 8 (2016) 24853–24861, https://doi.org/10.1021/acsami.6b06012.
[19] Y. Xie, S. Xu, Z. Xu, H. Wu, C. Deng, X. Wang, Interface-mediated extremely low thermal conductivity of graphene aerogel, Carbon N. Y 98 (2016) 381–390, https://doi.org/10.1016/j.carbon.2015.11.033.
[20] X. Zhu, C. Yang, P. Wu, Z. Ma, Y. Shang, G. Bai, X. Liu, G. Chang, N. Li, J. Dai, X. Wang, H. Zhang, Precise control of versatile microstructure and properties of graphene aerogel: Via freezing manipulation, Nanoscale 12 (2020) 4882–4894, https://doi.org/10.1039/c9nr07861d.
[21] C. Yang, X. Zhu, X. Wang, J. Wang, H. Huang, Phase-field model of graphene aerogel formation by ice template method, Appl. Phys. Lett. 115 (2019), 111901, https://doi.org/10.1063/1.5120311.

[22] W. Zhan, S. Yu, L. Gao, F. Wang, X. Fu, G. Sui, X. Yang, Bioinspired assembly of carbon nanotube into graphene aerogel with "cabbagelike" hierarchical porous structure for highly efficient organic pollutants cleanup, ACS Appl. Mater. Interfaces 10 (2018) 1093–1103, https://doi.org/10.1021/acsami.7b15322.
[23] Y. Xu, K. Sheng, C. Li, G. Shi, Self-assembled graphene hydrogel via a one-step hydrothermal process, ACS Nano 4 (2010) 4324–4330, https://doi.org/10.1021/nn101187z.
[24] L. Qiu, J.Z. Liu, S.L.Y. Chang, Y. Wu, D. Li, Biomimetic superelastic graphene-based cellular monoliths, Nat. Commun. 3 (2012) 1–7, https://doi.org/10.1038/ncomms2251.
[25] Z. Wang, R. Wei, J. Gu, H. Liu, C. Liu, C. Luo, J. Kong, Q. Shao, N. Wang, Z. Guo, X. Liu, Ultralight, highly compressible and fire-retardant graphene aerogel with self-adjustable electromagnetic wave absorption, Carbon N. Y. 139 (2018) 1126–1135, https://doi.org/10.1016/j.carbon.2018.08.014.
[26] H. Wang, C. Wang, S. Liu, L. Chen, S. Yang, Superhydrophobic and superoleophilic graphene aerogel for adsorption of oil pollutants from water, RSC Adv. 9 (2019) 8569–8574, https://doi.org/10.1039/c9ra00279k.
[27] J. Wang, X. Duan, Q. Dong, F. Meng, X. Tan, S. Liu, S. Wang, Facile synthesis of N-doped 3D graphene aerogel and its excellent performance in catalytic degradation of antibiotic contaminants in water, Carbon N. Y. 144 (2019) 781–790, https://doi.org/10.1016/j.carbon.2019.01.003.
[28] Y. Song, H. Li, Y. Gao, Q. Yue, B. Gao, W. Kong, Y. Zang, W. Jiang, Grass-modified graphene aerogel for effective oil-water separation, Process Saf. Environ. Prot. 129 (2019) 119–129, https://doi.org/10.1016/j.psep.2019.06.018.
[29] J.Y. Hong, E.H. Sohn, S. Park, H.S. Park, Highly-efficient and recyclable oil absorbing performance of functionalized graphene aerogel, Chem. Eng. J. 269 (2015) 229–235, https://doi.org/10.1016/j.cej.2015.01.066.
[30] N. Li, Q. Yue, B. Gao, X. Xu, R. Su, B. yu, One-step synthesis of peanut hull/graphene aerogel for highly efficient oil-water separation, J. Clean. Prod. 207 (2019) 764–771, https://doi.org/10.1016/j.jclepro.2018.10.038.
[31] H. Hu, Z. Zhao, W. Wan, Y. Gogotsi, J. Qiu, Ultralight and highly compressible graphene aerogels, Adv. Mater. 25 (2013) 2219–2223, https://doi.org/10.1002/adma.201204530.
[32] D.C. Marcano, D.V. Kosynkin, J.M. Berlin, A. Sinitskii, Z. Sun, A. Slesarev, L. B. Alemany, W. Lu, J.M. Tour, Improved synthesis of graphene oxide, ACS Nano 4 (2010) 4806–4814, https://doi.org/10.1021/nn1006368.
[33] G.E.P. Box, D.W. Behnken, Some new three level designs for the study of quantitative variables, Technometrics 2 (1960) 455–475, https://doi.org/10.1080/00401706.1960.10489912.
[34] R.V. Lenth, Response-surface methods in R, using RSM, J. Stat. Softw. 32 (2009) 1–17, https://doi.org/10.18637/jss.v032.i07.
[35] F. Menges, Spectragryph - optical spectroscopy software, (n.d.). http://www.effemm2.de/spectragryph/.
[36] M. Acik, G. Lee, C. Mattevi, A. Pirkle, R.M. Wallace, M. Chhowalla, K. Cho, Y. Chabal, The role of oxygen during thermal reduction of graphene oxide studied by infrared absorption spectroscopy, J. Phys. Chem. C. 115 (2011) 19761–19781, https://doi.org/10.1021/jp2052618.
[37] A. Duralliu, P. Matejtschuk, D.R. Williams, Measuring the specific surface area (SSA) of freeze-dried biologics using inverse gas chromatography, Eur. J. Pharm. Biopharm. 142 (2019) 216–221, https://doi.org/10.1016/j.ejpb.2019.06.026.
[38] J. Cai, J. Tian, H. Gu, Z. Guo, Amino carbon nanotube modified reduced graphene oxide aerogel for oil/water separation, ES Mater. Manuf. 6 (2019) 68–74, https://doi.org/10.30919/esmm5f611.
[39] S.P. Lee, G.A.M. Ali, H.H. Hegazy, H.N. Lim, K.F. Chong, Optimizing reduced graphene oxide aerogel for a supercapacitor, Energy Fuels. 35 (2021) 4559–4569, https://doi.org/10.1021/acs.energyfuels.0c04126.
[40] H. Geng, X. Liu, G. Shi, G. Bai, J. Ma, J. Chen, Z. Wu, Y. Song, H. Fang, J. Wang, Graphene oxide restricts growth and recrystallization of ice crystals, Angew. Chem. Int. Ed. 56 (2017) 997–1001, https://doi.org/10.1002/anie.201609230.
[41] Z. Zhang, H. Huang, X. Yang, L. Zang, Tailoring electronic properties of graphene by π-π stacking with aromatic molecules, J. Phys. Chem. Lett. 2 (2011) 2897–2905, https://doi.org/10.1021/jz201273r.
[42] D.R. Dreyer, S. Park, C.W. Bielawski, R.S. Ruoff, The chemistry of graphene oxide, Chem. Soc. Rev. 39 (2010) 228–240, https://doi.org/10.1039/b917103g.
[43] M. Pérez-Mendoza, M.C. Almazán-Almazán, L. Méndez-Liñán, M. Domingo-García, F.J. López-Garzón, Evaluation of the dispersive component of the surface energy of active carbons as determined by inverse gas chromatography at zero surface coverage, J. Chromatogr. A 1214 (2008) 121–127, https://doi.org/10.1016/j.chroma.2008.10.070.
[44] C. Niu, W. Xia, Y. Peng, Analysis of coal wettability by inverse gas chromatography and its guidance for coal flotation, Fuel 228 (2018) 290–296, https://doi.org/10.1016/j.fuel.2018.04.146.
[45] U. Mayer, V. Gutmann, W. Gerger, The acceptor number - a quantitative empirical parameter for the electrophilic properties of solvents, Mon. Chem. 106 (1975) 1235–1257, https://doi.org/10.1007/BF00913599.
[46] M.H. Abraham, Scales of solute hydrogen-bonding: their construction and application to physicochemical and biochemical processes, Chem. Soc. Rev. 22 (1993) 73–83, https://doi.org/10.1039/CS9932200073.
[47] C.F. Poole, S.K. Poole, Column selectivity from the perspective of the solvation parameter model, J. Chromatogr. A 965 (2002) 263–299, https://doi.org/10.1016/S0021-9673(01)01361-9.